RSC Advances

RSC Publishing

PAPER

View Article Online
View Journal

Controlled synthesis of low polydispersity Ag@SiO_2 core–shell nanoparticles for use in plasmonic applications

Cite this: DOI: 10.1039/c3ra41677a

Luc Rainville, Marie-Christine Dorais and Denis Boudreau*

A novel methodology was developed for the synthesis of tuneable silver–silica core–shell nanoparticles (Ag@SiO_2). The use of tannic acid and sodium citrate to reduce and stabilize silver atoms allowed the controlled synthesis of silver cores ranging from 26–118 nm in diameter, and silica shells of tuneable thicknesses from 6–51 nm were deposited using a combination of tetraethyl orthosilicate and sodium citrate. Both core size and spacer thickness can be tuned over a wide range of diameters and thicknesses by the simple variation of the reagent stoichiometric ratios, and mg range quantities of highly uniform core–shell nanoparticles can be prepared with excellent repeatability and reproducibility. To ascertain the usefulness of the core–shell nanoparticles for plasmonic enhancement studies, fluorescence measurements were performed on core–shell and coreless nanoparticles coated with a molecular fluorophore.

Received 8th April 2013,
Accepted 15th May 2013

DOI: 10.1039/c3ra41677a

www.rsc.org/advances

Introduction

Nanoparticle studies vary wildly in scope, covering both organic[1–3] and inorganic[4–7] syntheses and their subsequent applications. Plasmonics is a subset of this field, brought in by the distinctive electrical and photophysical characteristics of conductive nanoparticles and nanomaterials. A particularly noteworthy property of localized plasmons is the alteration of emissive electromagnetic processes *via* the generation of intense, localized electric fields.[8] For example, the enhancement of Raman scattering[9–13] and molecular luminescence[14–20] by plasmonic nanoparticles has been studied extensively for the purpose of qualitative and quantitative chemical analysis.[21–26] Other important applications of localized plasmons include photocatalysis[27–30] (*e.g.*, water splitting) and solar photovoltaics.[31–33]

The extent of plasmonic enhancement in photophysical and photochemical processes is often related to nanoparticle composition, size and shape;[34] consequently, a wide array of nanoparticle shapes has been investigated, from spheres to more complex shapes like cubes and octahedrons, as well as nanorods and nanowires of varying lengths.[34,35] Moreover, because plasmonic enhancement depends strongly on the metal substrate, a plethora of metals providing different plasmon resonant frequencies and enhancement factors have been investigated. The most popular metals to date have been gold and silver, due to their plasmon resonance bands located in the visible region of the electromagnetic spectrum, with silver providing the strongest enhancement due to its higher permittivity.[36]

The synthesis of metal nanoparticles can be fairly simple, and methods for doing so have been known for a long time. The challenge arises when trying to synthesize nanoparticles with uniform and specific shapes and sizes. Several research groups have investigated different approaches to achieve this goal.[37–43] The importance of this control is two-fold. To begin with, controlling particle morphology is important in radiative decay engineering studies when trying to correlate specific plasmon properties to radiative behavior, *i.e.*, correlating a particular behavior to a specific plasmon feature is impossible when the studied samples contain a heterogeneous population of nanoparticles. Single-particle studies[44] are another way to circumvent such synthetic limitations. Moreover, real-world applications have requirements and limitations that need to be met. A high degree of control and predictability means that particles can be quickly and efficiently adapted to suit specific needs.

Finally, in addition to the need for uniform nanoparticle size and shape, it is known that plasmonic enhancement also depends strongly on the distance of the chemical species or process being affected relative to the metal surface.[36] Coating nanoparticles with silica layers provides a convenient means to control this spacing in multilayer nanoparticle design,[45] in addition to limiting aggregation and providing a host of robust chemistries for predictable and reproducible functionalization of the nanoparticle surface.[45] Stöber[46] brought about the general method for condensing organic silicates into particles in alcohol–water mixtures, and this methodology was later adapted to the formation of mesoporous silica shells over

Department of Chemistry and Centre d'Optique, Photonique et Laser (COPL), Université Laval, Quebec City, QC, Canada G1V 0A6.
E-mail: denis.boudreau@chm.ulaval.ca

silica cores[47] and more recently expanded by Blaaderen[48] to form silica shells over a range of different colloidal cores. Nevertheless, adapting this simple and elegant method to a specific nanoparticle synthesis while controlling particle morphology and polydispersity is not straightforward, as shell-forming silica condensation is sensitive to a host of factors including pH, temperature, solvent, surface chemistry, and of course the silane precursor.

The work discussed herein describes a procedure for the facile synthesis of sizable quantities of $Ag@SiO_2$ core–shell nanoparticles with narrow, reproducible size distributions and morphologies over a wide range of sizes. Notably, this is the first reported synthesis of a silica shell over silver nanoparticles produced using tannic acid as the reducing agent. This synthetic methodology was designed to offer optimal control of nanoconstruct morphology in as few steps as possible. To ascertain the efficacy of core–shell nanoparticles fabricated using this method for plasmonic enhancement studies, fluorescence measurements were performed on core–shell nanoparticles and nanoshells (*i.e.*, coreless nanoparticles) coated with a molecular fluorophore.

Experimental

Chemicals and reagents

Tannic acid, sodium citrate tribasic (99.0% ACS Reagent), polyvinylpyrrolidone (PVP10, M_w 10 000), 2-(*N*-morpholino)ethanesulfonic acid (MES) hydrate ($\geqslant$99.5%) and ammonium hydroxide (28–30% NH_3) were purchased from Sigma-Aldrich. Tetraethyl orthosilicate (TEOS, 99.9%) and (3-aminopropyl)triethoxysilane (APTES, 98%) were purchased from Alfa Aesar. Silver nitrate (99.9995%) was purchased from Strem Chemicals, anhydrous ethanol from Commercial Alcohols, eosin-5-isothiocyanate (EiTC) from Marker Gene Technologies and potassium cyanide (>98.0%) from Fluka. The MES buffer solution (11.2 mM, pH 6.5) was prepared using MES hydrate and sodium hydroxide (ACS > 97.0%, BDH). All reagents were used as received, except for EiTC which was divided into 185 μg freeze–dried aliquots prior to use. Ultrapure water (18.2 MΩ) was used in all experimental processes as needed, unless specified otherwise. All glassware was washed with concentrated nitric acid, and then rinsed thoroughly with water.

Synthesis of silver nanoparticles

This synthesis is an expanded, scaled up version of the work of Dadosh.[49] 90 mg of $AgNO_3$ (1.32 mM) is dissolved in 400 mL of water. Another 100 mL aqueous solution is prepared containing 250 mg of tannic acid (1.47 mM) and 360 mg of citrate (12.2 mM). Both mixtures are heated to 60 °C before being combined together under vigorous stirring. After being kept at 60 °C for 5 min, the solution is brought to the boil for 20 min, then left to cool. The resulting mixture is centrifuged twice (11 000 RCF, 60 min) and dispersed in 350 mL of water. This suspension is then mixed with 468 mg of PVP10 diluted in 25 mL of water. PVP is used as a surface priming agent to be covered or displaced by the silica shell. The quantity added is calculated considering the target surface density (60 molecules nm^{-2}) suggested by Blaaderen.[48] The total surface is calculated assuming 100% Ag reduction yield, perfect spherical shape, and a silver core density of 10.49 g cm^{-3}. This mixture is left to react for a minimum of 12 h at 30 °C under stirring, followed by two centrifugations (11 000 RCF, 60 min). The resulting PVP-coated nanoparticles are finally dispersed in 350 mL of water. This particular set of concentrations typically yields silver nanoparticles with an average core diameter of 55–60 nm.

Synthesis of silica spacer shell

Reaction conditions are based on the Blaaderen[48] method, with the exception of sodium citrate usage, as described below. Various amounts of aqueous sodium citrate (26.6 mM) are added to 100 mL aliquots of silver nanoparticle solution and diluted to a final volume of 120 mL to yield citrate concentrations of 1.11, 2.22 and 3.33 mM. These are left to stir overnight at 30 °C. Four 25 mL aliquots are extracted from every mix. To each is then added 100 mL of anhydrous ethanol, 10–34 μL of TEOS (0.41–1.4 mM) and, 5 min later, 1 mL NH_4OH. After these solutions have been left to react for 24 h at 30 °C under stirring, the nanoparticles are centrifuged three times (14 000 RCF, 20 min) and dispersed each time in anhydrous ethanol, for a final volume of 50 mL. It was observed that the reaction conditions sometimes lead to a slight reduction in the silver core sizes. Core–shell cores retain, on average, >90% of their diameter after purification when compared to the initial silver nanoparticle suspension.

Fluorescent labeling of $Ag@SiO_2$ core–shell nanoparticles

This step was adapted from our previous work.[15] 620 μL of a 1.43 mM solution of APTES in ethanol is added to 185 μg of EiTC (0.43 mM). This mixture is left to react for 4 h at room temperature under agitation. This fluorophore–silane precursor mixture is added to 10 mL aliquots of $Ag@SiO_2$ nanoparticles in concentrations ranging from 0–3.38 μM (0–80 μL in 10 mL) followed by the addition of 240 μL of concentrated NH_4OH and, a few minutes later, 300 μL of a 0.22% (v/v) TEOS solution. The TEOS will co-condense with the silane coupling agent and form a second, fluorophore-enriched shell. These nanoparticles are centrifuged (14 000 RCF, 20 min), discarding the supernatant and suspending them in anhydrous ethanol. This step is repeated until fluorescence measurements indicate no detectable traces of the fluorophore in the supernatant.

Evaluation of fluorescence enhancement factor (EF)

The extent of fluorescence enhancement achieved with $Ag@SiO_2@SiO_2$–eosin nanoparticles was quantified by comparing the steady-state fluorescence intensity of dye-doped core–shell and coreless (shell only) nanoparticles. The core–shell samples were prepared by diluting 120 μL of dye-doped nanoparticle solution in 10 mL of MES buffer (11.2 mM, pH 6.5). The coreless samples were prepared by adding 70 μL of 0.1 M $KCN_{(aq)}$ to 7 mL of this buffered nanoparticle solution and left for 24 h to dissolve the silver cores before taking fluorescence measurements of the resulting solution.

Monitoring the plasmon intensity by UV-Vis after the addition of cyanide showed a rapid decrease in plasmon band intensity while undergoing a blue shift, indicating smaller average metal core diameters until none could be detected. Measurements on a buffered eosin solution confirmed that 1 mM cyanide has no noticeable effect on fluorescence intensity or lifetime. Because of the lower sensitivity of the fluorescence lifetime platform used in this work, more concentrated nanoparticle samples were prepared for the time-resolved fluorescence measurements. The core–shell samples were prepared by adding 500 μL of dye-doped nanoparticles to 5 mL of MES buffer, with corresponding nanoshells obtained from the latter by spiking with 50 μL 0.1 M $KCN_{(aq)}$. Measurements were taken after 24 h to ensure complete etching of the plasmonic cores. The instrument response function (IRF) was acquired using $Ag@SiO_2$ nanoparticles as the scatterer.

Nanoparticle characterization

Transmission electron microscopy (TEM, Phillips Tecnai 12) was used to evaluate the size, morphology, and structure of the core–shell nanoparticles. Nanoparticle samples were prepared on carbon films supported by copper hexagonal 200 mesh grids (Canemco). TEM images were processed using commercial image analysis software (IMT i-Solution). Steady-state fluorescence measurements were performed on a high-end spectrofluorometer (Fluorolog 3–22 with R928 PMT detector, Horiba). Fluorescence lifetime data was obtained with a time-resolved fluorescence platform (FluoTime 200, PicoQuant GmbH) equipped with a 485 nm pulsed laser (LDH-P-C-485, PicoQuant GmbH). Repetition rate for the laser was 10 MHz, and the detector monochromator was set to 540 nm. Fluorescence lifetimes were extracted from the decay curves using commercially available fluorescence lifetime analysis software (FluoFit Pro, PicoQuant GmbH). UV-Vis extinction spectra were measured on a Varian Cary 50 spectrophotometer (200–800 nm).

Results and discussion

Using tannic acid as a reducer, we were able to produce ~50 mg batches of PVP10-coated silver nanoparticles with controllable sizes ranging from 26–118 nm in diameter. The various sets of experimental conditions used to cover this range are presented in Table 1. The corresponding extinction spectra and TEM images, along with size distribution histograms are shown in Fig. 1 and 2, respectively. For all syntheses, the RSD calculated on the diameter was below 15%. The samples were stable for months when stored in the dark at 20 °C.

Table 1 Characterization data and reagent concentrations for Ag nanoparticles with core diameters 26–118 nm

	A	B	C	D	E	F
Diameter (nm)	26	33	40	59	96	118
RSD (%)	10	10	14	13	14	9
Citrate (mM)	12.2	12.2	12.2	12.2	1.70	1.53
Tannic acid (μM)	24	47	290	1460	1110	1760
λ_{max} (nm)	395	398	409	433	484	507

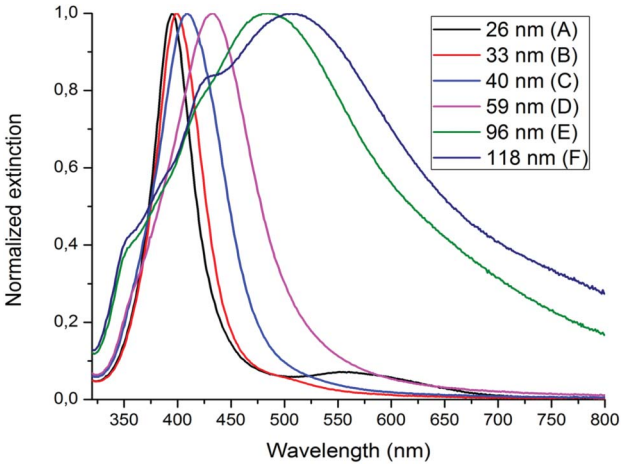

Fig. 1 Normalized extinction spectra for Ag nanoparticle samples A–F (see Table 1).

Control over the nanoparticle size was achieved by altering the tannic acid and sodium citrate concentrations. It was suggested by Santhanam[50] that the concentration of tannic acid dictates the rate and extent of nucleation, with lower concentrations favoring fast nucleation and smaller particles. This would be the case because tannic acid acts not only as a reducing agent, but also as a ligand (through gallic acid monomers) for silver atoms. As the tannic acid concentration is lowered, the average number of silver atoms per tannic acid molecule increases, favoring nucleation over growth. Conversely, as the ratio is shifted to fewer silver atoms per tannic acid, the nucleation rate between silver atoms is lowered. Nanoparticles increase in size with increasing tannic acid concentration, for a fixed citrate concentration. This synthesis follows this trend, as seen in Fig. 3. Sodium citrate influences particle size in the opposite way, with higher concentrations leading to smaller particles for a fixed tannic acid concentration. This is consistent with the reported role of citrate as surface-stabilizing agent.[37,38] By tuning both the citrate and tannic acid concentrations, it is possible to obtain silver nanoparticles with specific sizes in a repeatable fashion.

Silver nanoplates could be observed alongside the larger particles (Fig. 2F). Such structures appear more abundant as the reagent concentrations are adjusted to yield bigger nanoparticles. The nanoplates account for roughly 8% of the nanoparticle count in the images (N = 1600), but arguably less of the mass of the sample because of their planar shape. This has been observed in all syntheses yielding nanoparticles 90 nm in diameter or larger.

The repeatability of the method was evaluated by comparing several samples prepared at different times over a one year span, using two distinct sets of reaction parameters. The resulting average particle size for samples prepared using parameter set A (12.2 mM citrate, 1.11 mM tannic acid) is 44

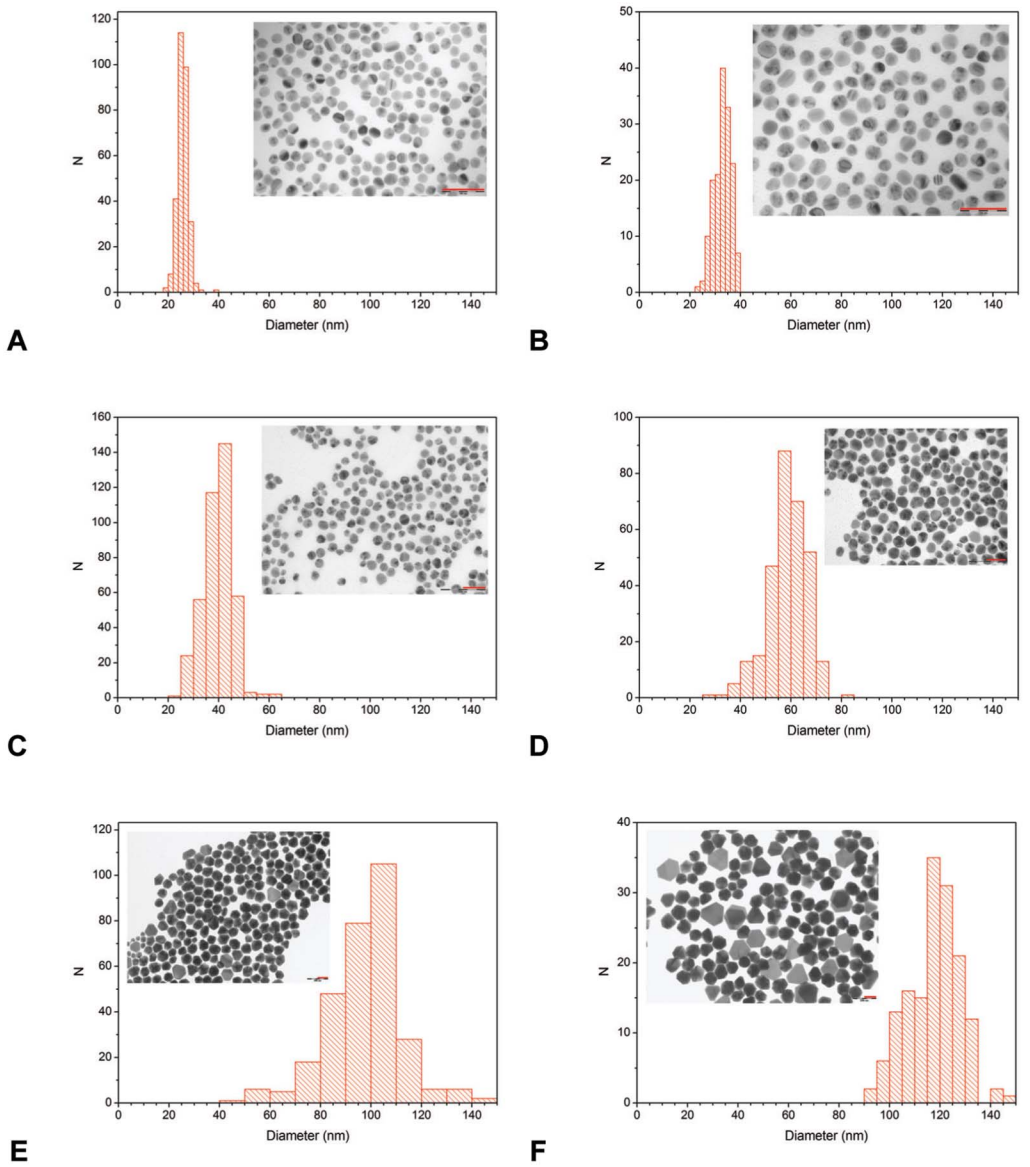

Fig. 2 TEM images and size distribution histograms for Ag nanoparticles described in Table 1. Red scale bars represent 100 nm.

nm with a RSD of 3.7%, while the average particle size for parameter set B (12.2 mM citrate, 1.47 mM tannic acid) samples is 57 nm with a RSD of 2.9%. As shown in Fig. 4 (top), the extinction spectra for the samples in each set are very similar, with average plasmon band central peak wavelengths of 420 $\pm$ 2 nm and 430 $\pm$ 2 nm, and bandwidths (FWHM) of 81 $\pm$ 4 nm and 93 $\pm$ 7 nm for sets A and B, respectively. This is very convincing evidence of a very good repeatability of the achieved average diameter and polydispersity for these reaction conditions.

The reproducibility of the method was evaluated by supplying four people with instructions to synthesize silver nanoparticles using parameter set A without prior knowledge of the methodology. As shown by the extinction spectra in Fig. 4 (bottom), the optical extinction spectra of the nanoparticles remain constant regardless of who performed the synthesis with a given set of reaction parameters, with an average plasmon band central peak wavelength of 417 $\pm$ 1 nm and a bandwidth (FWHM) of 86 $\pm$ 4 nm.

The key to controlling the thickness of the silica coating on tannic acid prepared nanoparticles resides in the addition of sodium citrate alongside the silica precursor. The effect of citrate on the thickness of condensed silica as a function of TEOS concentration was investigated for various core sizes, and silica shells were fabricated with tuneable thicknesses ranging from 6–51 nm (Fig. 5). Table 2 shows the relationship between TEOS concentration, citrate concentration and silica shell thickness for core sizes ranging from 33–96 nm. Fig. 6 (top) shows the increase in shell thickness due to increasing citrate concentration from 1.11–3.33 mM for two fixed TEOS concentrations. This study unambiguously shows the influence of citrate on the formation of the silica coatings. For every

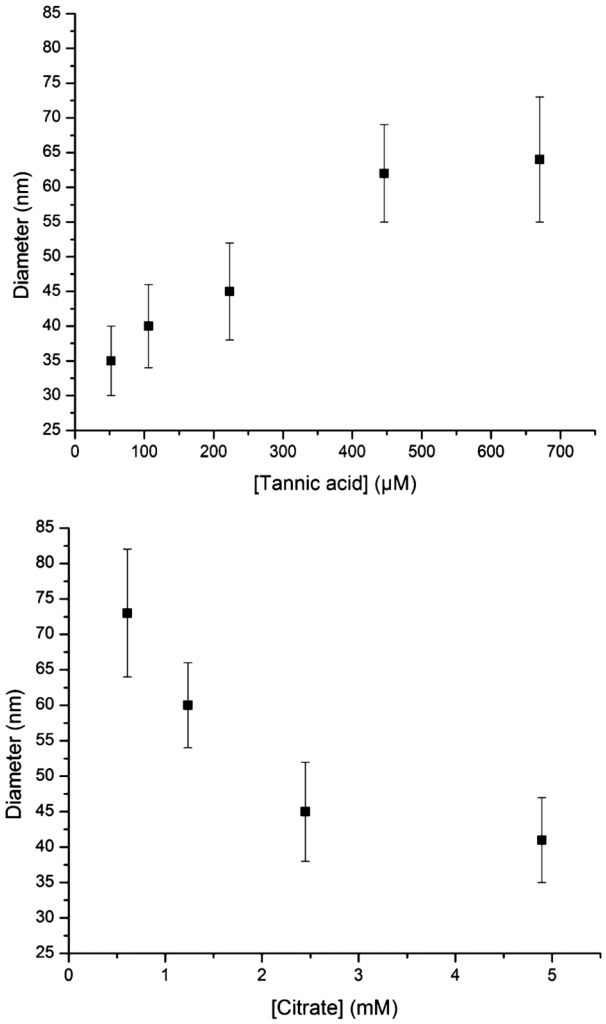

Fig. 3 Effect of varying concentrations of tannic acid (top, 12.2 mM sodium citrate) and sodium citrate (bottom, 222 μM tannic acid) on silver core diameter (all other parameters are kept constant).

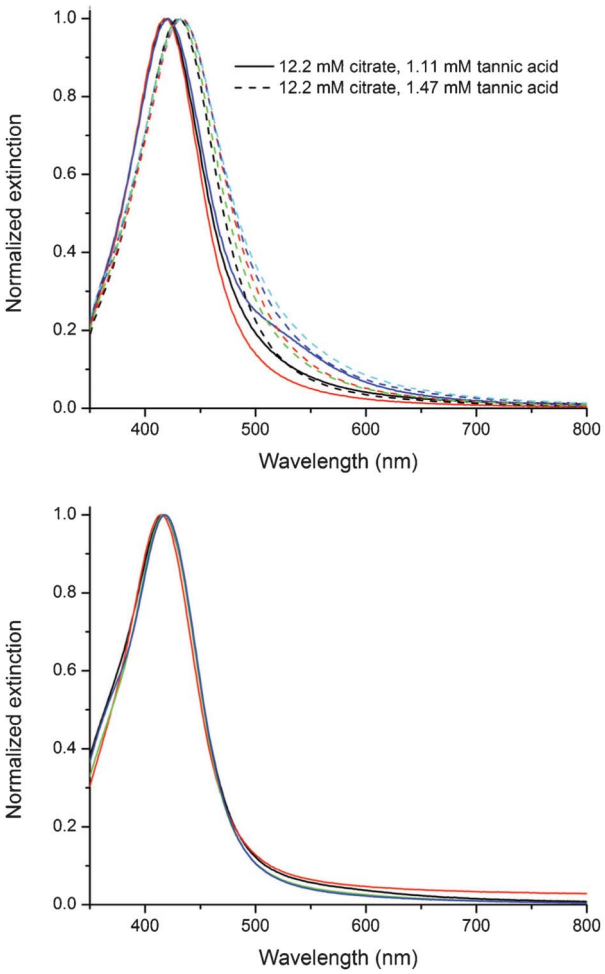

Fig. 4 Evaluation of repeatability (top) and reproducibility (bottom) of normalized extinction spectra from several nanoparticle samples.

silver core size, the use of a low (1.11 mM) citrate concentration leads to the condensation of thinner silica coatings at equivalent TEOS concentrations. On the other hand, the reaction without added citrate leads to thin (~5 nm) or incomplete silica shells, regardless of TEOS, ammonia or nanoparticle concentrations. As a rule, increasing the concentration of sodium citrate, for a given TEOS concentration, leads to greater shell thicknesses, albeit with a less marked difference observed between 2.22 and 3.33 mM. For all citrate concentrations studied, increasing the TEOS concentration leads to an increase in shell thickness (Fig. 6, bottom).

The goal behind this work is to create a platform providing stable and controllable geometry for the study and use of plasmon-altered processes in composite nanoparticles. To test the suitability of the as-prepared core-shell $Ag@SiO_2$ nanoparticles as potential fluorescence enhancers, a series of dye-doped core–shells were synthesized. Their core sizes ranged from 29–99 nm with coatings from 6–10 nm in thickness. The resulting fluorescence data is presented in Fig. 7 and Table 3.

Emission enhancement was observed for the samples with 38, 55 and 99 nm core diameters, *i.e.*, the fluorescence intensity from core–shell nanoparticles were stronger than from their coreless counterparts. These findings were confirmed by fluorescence lifetime measurements, with plasmon-enhanced eosin emission exhibiting average lifetimes of 210 ps or less, much shorter than eosin's lifetime of 1.11 ns when free in solution. Interestingly, since the photostability of fluorophores depends, among other factors, on the lifetime of their excited states, these $Ag@SiO_2@SiO_2$–dye core–shell nanocomposites

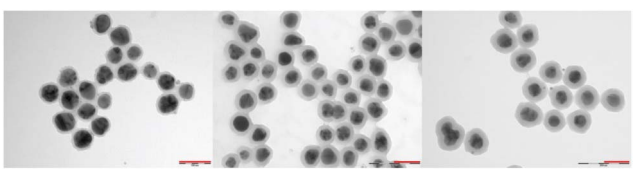

Fig. 5 TEM images of $Ag@SiO_2$ nanoparticles with average core size of 54 nm and increasing silica shell thicknesses (7, 13, 21 nm left to right). Red scale bars represent 100 nm.

Table 2 Data showing the relation between TEOS concentration and silica shell thickness for varying concentrations of sodium citrate and core sizes

		Core diameter (nm)							
		33		40		59		96	
Citrate (mM)	TEOS (mM)	d_{SiO2} (nm)	RSD (%)	d_{SiO2} (nm)	RSD (%)	d_{SiO2} (nm)	RSD (%)	d_{SiO2} (nm)	RSD (%)
1.11	0.41	6.4	14	7	21	6.2	13	9	23
	0.74	9	16	10	18	12	12	11	16
	1.07	12	16	14	14	14	15	14	12
	1.40	12	17	16	13	15	12	24	14
2.22	0.41	9	13	8	16	8	13	12	18
	0.74	17	15	19	17	20	11	29	7
	1.07	21	11	29	11	25	14	37	9
	1.40	25	9	34	13	26	10	40	18
3.33	0.41	10	14	11	13	9	16	17	9
	0.74	19	11	19	12	22	9	38	8
	1.07	21	10	26	10	33	9	51	8
	1.40	28	8	30	9	38	9	40	7

should display enhanced robustness toward photodestructive processes and thereby giving a substantial increase in number of emitted photons.[15] Furthermore, the highest enhancement factor (4.6) was measured for the 55 nm sample, which falls within the 40–70 nm range for optimal fluorescent enhancement for silver nanoparticles according to Lakowicz.[14] On the other hand, eosin emission was lower in the 29 nm core–shell sample (E.F. = 0.18), possibly due to the thinner spacer

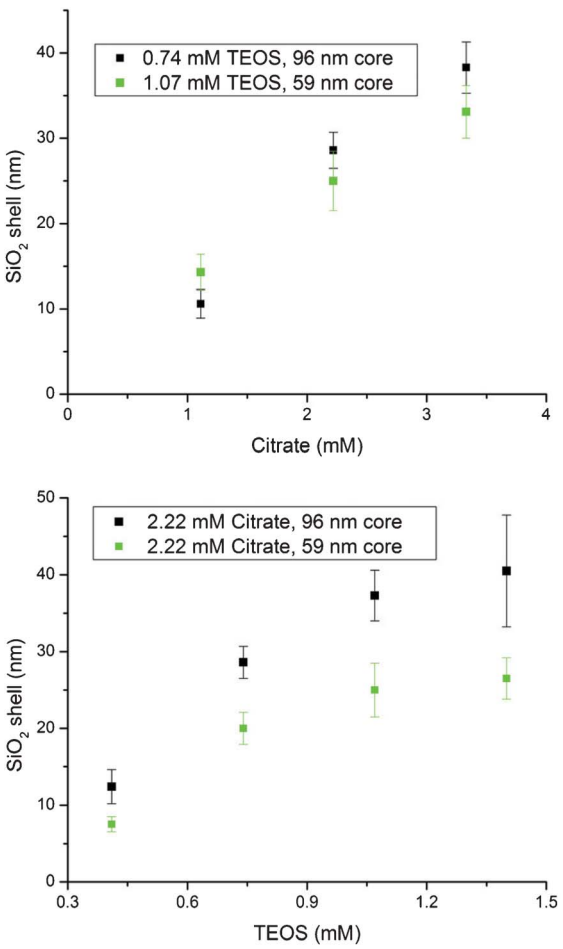

Fig. 6 Thickness of silica shell coating on 59 and 96 nm Ag cores for varying citrate (top) and TEOS concentrations (bottom).

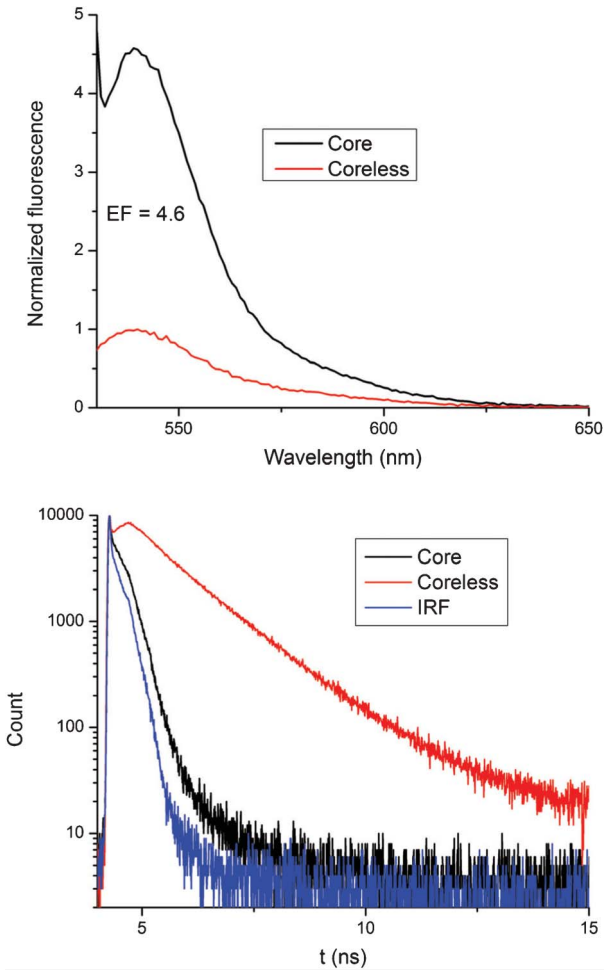

Fig. 7 Steady-state fluorescence spectra (top) and fluorescence lifetime decay curves (bottom) for eosin coated core–shell and coreless nanoparticles (55 nm core, 8 nm shell).

Table 3 Fluorescence, enhancement factor, and lifetime data for core–shell (top row) and coreless (bottom row) for given sets of $Ag@SiO_2$ nanoparticles[a]

Core (nm)	Shell (nm)	Fluo (10^5 CPS)	E.F.	τ_{ave} (ns)	τ_1 (ns)	A_1	τ_2 (ns)	A_2	$\chi 2$
29 ± 3	6 ± 1	0.54	0.18	0.43	0.23	198	1.36	43	1.000
		2.90		1.33	1.19	4138	3.85	230	0.980
38 ± 4	8 ± 1	10.6	2.6	0.21	0.19	2096	0.61	118	1.001
		4.04		1.18	1.06	1135	2.27	123	1.078
55 ± 7	8 ± 1	11.4	4.6	0.19	0.19	1023			1.086
		2.47		1.22	1.16	8511	4.17	171	1.001
99 ± 9	10 ± 2	4.22	1.8	0.13	0.11	882	0.85	26	1.078
		2.35		1.27	1.14	3806	3.81	187	1.046

[a] Average fluorescence lifetimes were calculated by fitting the decay curves with a double exponential of the form $\tau_{ave} = (\tau_1 \times A_1 + \tau_2 \times A_2)/(A_1 + A_2)$, where τ and A are the lifetime and amplitude values, respectively.

allowing the fluorophore to creep too close to the metallic core in the porous silica matrix, thus promoting quenching over emission enhancement.[18]

Conclusion

In this work, we were able to fabricate, using a versatile, simple, and reproducible procedure, a core–shell nanoarchitecture featuring a silver core surrounded by a concentric silica layer acting as a spacer between the core and outlying molecular fluorophores. The pivotal innovation in this procedure is that both the core size and the spacer thickness can be tuned over a wide range of diameters and thicknesses by the simple variation of the reagent stoichiometric ratios, so that the geometry of the nanocomposites can easily be adapted for maximum plasmonic enhancement of photophysical or photochemical processes.

The comparison of photophysical characteristics of fluorophore-coated core–shell and coreless nanostructures with similar geometry shows that the luminosity and radiative decay rate of the surrounding fluorophores are increased several fold by the metal-enhanced fluorescence displayed by the core–shell nanocomposites. The improved photophysical properties of such tailored metal@dielectric nanocomposites could be useful for many plasmonic applications, including biosensor design, intracellular chemical imaging, and plasmonic enhancement of solar photovoltaic devices.

Acknowledgements

We are grateful to the Natural Sciences and Engineering Research Council of Canada, the ''Fonds pour la Recherche du Québec-Nature et Technologies'' and the Canada Foundation for Innovation for financial support of this work. The authors would also like to express their gratitude to Marie-France Champigny of the ''Institut Universitaire en Santé Mentale de Québec'' and Marc Choquette of the ''Laboratoire de Microanalyse de l'Université Laval'' for help with TEM sample preparation and characterization, and to Samuel Ouellet and Félix-Antoine Lavoie for assistance with lifetime measurements.

References

1 S. Chen, W. Qin, Z. Zhao, B. Z. Tang and H.-S. Kwok, *J. Mater. Chem.*, 2012, **22**, 13386.
2 P. Guo, C. R. Martin, Y. Zhao, J. Ge and R. N. Zare, *Nano Lett.*, 2010, **10**, 2202–2206.
3 I. Milošević, V. Mauroy, H. Dabboue, S. Serieye, F. Warmont, J.-P. Salvetat, M.-L. Saboungi and S. Guillot, *Microporous Mesoporous Mater.*, 2009, **120**, 7–11.
4 A. Valizadeh, H. Mikaeili, M. Samiei, S. M. Farkhani, N. Zarghami, M. Kouhi, A. Akbarzadeh and S. Davaran, *Nanoscale Res. Lett.*, 2012, **7**, 480.
5 G. Chen, H. Qiu, R. Fan, S. Hao, S. Tan, C. Yang and G. Han, *J. Mater. Chem.*, 2012, **22**, 20190.
6 N. Insin, J. B. Tracy, H. Lee, J. P. Zimmer, R. M. Westervelt and M. G. Bawendi, *ACS Nano*, 2008, **2**, 197–202.
7 Z. Ma, D. Dosev, M. Nichkova, R. K. Dumas, S. J. Gee, B. D. Hammock, K. Liu and I. M. Kennedy, *J. Magn. Magn. Mater.*, 2009, **321**, 1368–1371.
8 S. A. Maier, *Plasmonics: Fundamentals and Applications*, Springer Science, New York, 2007.
9 K. Zhang, Y. Xiang, X. Wu, L. Feng, W. He, J. Liu, W. Zhou and S. Xie, *Langmuir*, 2009, **25**, 1162–1168.
10 C. Fernandez-Lopez, C. Mateo-Mateo, R. A. Alvarez-Puebla, J. Perez-Juste, I. Pastoriza-Santos and L. M. Liz-Marzan, *Langmuir*, 2009, **25**, 13894–13899.
11 D. Li, S. Wu, Q. Wang, Y. Wu, W. Peng and L. Pan, *J. Phys. Chem. C*, 2012, **116**, 12283–12294.
12 M. Rycenga, X. Xia, C. H. Moran, F. Zhou, D. Qin, Z. Y. Li and Y. Xia, *Angew. Chem., Int. Ed.*, 2011, **50**, 5473–5477.
13 Y. Yang, S. Matsubara, L. Xiong, T. Hayakawa and M. Nogami, *J. Phys. Chem. C*, 2007, **111**, 9095–9104.
14 J. R. Lakowicz, *Anal. Biochem.*, 2005, **337**, 171–194.
15 M. Lessard-Viger, M. Rioux, L. Rainville and D. Boudreau, *Nano Lett.*, 2009, **9**, 3066–3071.
16 A. R. Guerrero, Y. Zhang and R. F. Aroca, *Small*, 2012, **8**, 2964–2967.
17 Y. Zhang, K. Aslan, M. J. Previte and C. D. Geddes, *Appl. Phys. Lett.*, 2008, **92**, 13905.
18 M. L. Viger, L. S. Live, O. D. Therrien and D. Boudreau, *Plasmonics*, 2008, **3**, 33–40.
19 J. T. van Wijngaarden, M. M. van Schooneveld, C. de Mello Donegá and A. Meijerink, *Europhys. Lett.*, 2011, **93**, 57005.
20 Q. Wang, F. Song, C. Ming, H. Zhao, J. Liu, C. Zhang, S. Lin and E. Y.-B. Pun, *J. Opt. Soc. Am. B*, 2011, **28**, 220.

21 S. S. Dasary, A. K. Singh, D. Senapati, H. Yu and P. C. Ray, *J. Am. Chem. Soc.*, 2009, **131**, 13806–13812.
22 L. Marsich, A. Bonifacio, S. Mandal, S. Krol, C. Beleites and V. Sergo, *Langmuir*, 2012, **28**, 13166–13171.
23 C. Wang, Y. Chen, T. Wang, Z. Ma and Z. Su, *Adv. Funct. Mater.*, 2008, **18**, 355–361.
24 M. L. Viger, D. Brouard and D. Boudreau, *J. Phys. Chem. C*, 2011, **115**, 2974–2981.
25 M. H. Chowdhury, K. Ray, S. K. Gray, J. Pond and J. R. Lakowicz, *Anal. Chem.*, 2009, **81**, 1397–1403.
26 L. Zhou, F. Ding, H. Chen, W. Ding, W. Zhang and S. Y. Chou, *Anal. Chem.*, 2012, **84**, 4489–4495.
27 Y. Qu and X. Duan, *Chem. Soc. Rev.*, 2013, **42**, 2568–2580.
28 A. Sheikh, A. Yengantiwar, M. Deo, S. Kelkar and S. Ogale, *Small*, 2013, DOI: 10.1002/smll.201202140.
29 E. Thimsen, F. Le Formal, M. Gratzel and S. C. Warren, *Nano Lett.*, 2011, **11**, 35–43.
30 Z. Liu, W. Hou, P. Pavaskar, M. Aykol and S. B. Cronin, *Nano Lett.*, 2011, **11**, 1111–1116.
31 H. A. Atwater and A. Polman, *Nat. Mater.*, 2010, **9**, 205–213.
32 H. Choi, W. T. Chen and P. V. Kamat, *ACS Nano*, 2012, **6**, 4418–4427.
33 L. Lu, Z. Luo, T. Xu and L. Yu, *Nano Lett.*, 2013, **13**, 59–64.
34 X. Lu, M. Rycenga, S. E. Skrabalak, B. Wiley and Y. Xia, *Annu. Rev. Phys. Chem.*, 2009, **60**, 167–192.
35 X. Ye, L. Jin, H. Caglayan, J. Chen, G. Xing, C. Zheng, V. Doan-Nguyen, Y. Kang, N. Engheta, C. R. Kagan and C. B. Murray, *ACS Nano*, 2012, **6**, 2804–2817.
36 J. R. Lakowicz, *Plasmonics*, 2006, **1**, 5–33.
37 A. Henglein and M. Giersig, *J. Phys. Chem. B*, 1999, **103**, 9533–9539.
38 Z. S. Pillai and P. V. Kamat, *J. Phys. Chem. B*, 2004, **108**, 945–951.
39 B. Wiley, T. Herricks, Y. Sun and Y. Xia, *Nano Lett.*, 2004, **4**, 1733–1739.
40 M. Chen, Y. G. Feng, X. Wang, T. C. Li, J. Y. Zhang and D. J. Qian, *Langmuir*, 2007, **23**, 5296–5304.
41 D. Long, G. Wu and S. Chen, *Radiat. Phys. Chem.*, 2007, **76**, 1126–1131.
42 K.-S. Chou and Y.-S. Lai, *Mater. Chem. Phys.*, 2004, **83**, 82–88.
43 J. N. Solanki and Z. V. P. Murthy, *Ind. Eng. Chem. Res.*, 2011, **50**, 12311–12323.
44 Y. Chen, K. Munechika and D. S. Ginger, *Nano Lett.*, 2007, **7**, 690–696.
45 G. T. Hermanson, *Bioconjugate Techniques*, Elsevier, Amsterdam, 2nd edn, 2008.
46 W. Stöber, A. Fink and E. Bohn, *J. Colloid Interface Sci.*, 1968, **26**, 62–69.
47 G. Büchel, K. K. Unger, A. Matsumoto and K. Tsutsumi, *Adv. Mater.*, 1998, **10**, 1036–1038.
48 C. Graf, D. L. J. Vossen, A. Imhof and A. van Blaaderen, *Langmuir*, 2003, **19**, 6693–6700.
49 T. Dadosh, *Mater. Lett.*, 2009, **63**, 2236–2238.
50 S. K. Sivaraman, I. Elango, S. Kumar and V. Santhanam, *Curr. Sci.*, 2009, **97**, 1055.

